PPPL-1990

UC20-F,G

226
5-31-83

PPPL-1990
Dr. 1447-8

I-9492

MODELING OF ICRF HEATING OF A TOKAMAK PLASMA

By

D.Q. Hwang, C.F.F. Karney, J.C. Hosea,
J.M. Hovey, C.E. Singer, and J.R. Wilson

MAY 1983

PLASMA
PHYSICS
LABORATORY

PRINCETON UNIVERSITY
PRINCETON, NEW JERSEY

PREPARED FOR THE U.S. DEPARTMENT OF ENERGY,
UNDER CONTRACT DE-AC02-76-CHO-3073.

PPPL--1990

DE83 012421

MODELING OF ICRF HEATING OF A TOKAMAK PLASMA

D.Q. Hwang, C.F.F. Karney, J.C. Hosea,

J.M. Hovey, C.E. Singer, and J.R. Wilson

Plasma Physics Laboratory, Princeton University

Princeton, New Jersey 08544

ABSTRACT

A model for wave propagation and absorption of the Ion Cyclotron Range of Frequencies (ICRF) has been constructed and fitted into the 1-D BALDUR transport code. The wave propagation is handled by ray tracing techniques. Wave absorption is calculated using the Fokker-Planck equation and quasilinear diffusion. The wave propagation and damping profiles are evolved in time according to the plasma evolution. A simulation of PLT hydrogen minority ICRF heating with a comparison to experimental data is given.

I. INTRODUCTION

Recent ICRF heating experiments on a number of tokamaks, such as PLT, TFR, JIPPT-II, and JFT-II, have demonstrated efficient ion and electron heating in the fundamental minority, the two-ion hybrid, and the second harmonic regimes.[1-5] The first direct measurement of minority ion heating was documented on PLT by using the mass discriminating charge exchange diagnostic to identify the energetic minority hydrogen distribution in a deuterium plasma.[1] The observed minority ion energy spectrum was found to be in good agreement with quasilinear diffusion theory. More recently, the central deuteron temperature in PLT has reached 3 keV through collisions with an rf heated energetic ^{3}He ion distribution which consists of 5% of the electron density and whose energy is as high as 200 keV. Moreover, the fusion power output of the 14.7 MeV protons from the D - ^{3}He + p(14.7 MeV) + ^{4}He reactions in these experiments is approaching 1 kW.

In the pure second harmonic heating of a hydrogen plasma, the observed bulk ion distribution is non-Maxwellian, as predicted by quasilinear theory.[6] Thus, one cannot depict the heating result by a thermal temperature, but rather by 2/3 of the averaged ion energy, $\langle E \rangle$. The averaged ion energy for the best heating case in PLT has reached over 4.5 keV which corresponds to an effective temperature, $T_{eff} = 2\langle E \rangle/3$, of 3.2 keV. It should be noted that the characteristics of a 3.2 keV thermal plasma can be quite different from a non-Maxwellian plasma. For example, the estimated fusion power output from D-D reactions for a deuterium plasma with T_{eff} = 3.2 keV is four times higher than the corresponding thermal plasma. Moreover, the confinement properties of these plasmas are not the same.

In order to understand the present experimental results as well as to develop theoretical models capable of extrapolating these results to future

confinement devices, a theoretical effort has been initiated to integrate the various wave coupling, propagation, and absorption theories into tokamak transport models. In this paper, we present the results of incorporating these wave models into the one-dimensional transport code, BALDUR.[7] The wave power deposition profile is recomputed in time as the plasma parameters evolve according to the transport code. For the sake of computational speed, various approximations and assumptions have been made throughout the calculations. The validity and limitations of these approximations are discussed and further improvements to the modeling are suggested. Finally, a direct comparison of the modeling results with recent PLT minority heating data is given as an example.

II. THE RF MODEL

The modeling of rf heating requires two interlocking calculations: (1) the determination of the rf fields throughout the devices and, (2) the determination of the power deposition into the various components of the plasma. The computed power deposition profiles for the plasma species serve as the input for the transport code to recompute the various plasma parameters and profiles.

A. The plasma

The plasma consists of an arbitrary number of ion species enabling the simulation of a variety of ICRF heating scenarios. All plasma properties are assumed to be toroidally axisymmetric, as required for the 1-D transport code. The q profile, $q(r)$, and the profiles of density and temperature of each species, $n_s(r)$ and $T_s(r)$, are arbitrary circularly symmetric functions of the minor radius, r. These functions are obtained by fitting cubic splines

to the data from BALDUR.

The magnetic field has a toroidal component $B_\phi = B_{\phi_o} R_o/R$ and poloidal component $B_\theta = B_\phi\, r/q\, R_o$, where R_o is the major radius of the magnetic axis, R is the distance to the axis of the machine, ϕ is the toroidal angle, and θ is the poloidal angle.

Each plasma species is initialized as an isotropic Maxwellian distribution $f_s(r,v)$ produced in the ohmic phase of the transport simulation. During the rf heating pulse, the background species are assumed to stay isotropic and Maxwellian with the temperature computed by BALDUR. The test species, on the other hand, are allowed to become non-Maxwellian (but still isotropic) as a result of the wave damping and Fokker-Planck calculations.

B. Wave propagation

The calculation of the coupling and the propagation of the rf wave fields from the antenna to the plasma core is divided into two parts. First, the wave coupling problem is handled by solving the fields near the antenna in a cold plasma with a cylindrical conducting wall. (This is handled by a separate code that is still under development.) The antenna modeling provides the initial conditions for the wave propagation calculation. These conditions are the position (r,θ), the wave vector components (m=poloidal mode number, n=toroidal mode number), and the rf power distribution on the antenna $P(r,\theta)$. The toroidal wave vector, k_ϕ, is determined from the Fourier spectrum of several loop antennae located at different toroidal positions.

The propagation of the wave fields throughout the plasma is calculated using ray tracing equations. A cylindrical coordinate system is used with coordinates R, z, and ϕ where z is the altitude above the equatorial plane.

In this way the ray tracing equations are well-behaved throughout the plasma. The wave numbers conjugate to the space coordinates are k_R, k_z, and n. Since the plasma is axisymmetric, n is a constant. In addition we assume that there is a rapid equilibration of all plasma quantities on a given flux surface; therefore, we do not need to solve for the ϕ coordinate. Thus we need only solve for the four quantities, R, k_R, z, and k_z.

The ray tracing equations[8] take the form $dR/dt = -(\partial D/\partial k_R)/(\partial D/\partial \omega)$, and similarly for z and the wave numbers. Here D is the dispersion relation, considered as a function of the six space and wave number coordinates and of the frequency ω. D is calculated from the full set of Maxwell's equations and the linearized multi-species fluid equations with a pressure term, ∇p_s, in the momentum equation. The fluid equations are obtained by taking moments of the Vlasov equation. The pressure p_s satisfies a polytropic equation of state $(p_s/p_{so}) = (n_s/n_{so})^{\gamma_s}$. (In the simulation we took $\gamma_e = 1$, $\gamma_i = 3$.)

Given the initial spatial coordinate (r,θ), the wave numbers (m and n), and the rf power content along the antenna from the modeling, Newton's method is then used to find the value of k_r which exactly solves the dispersion relation. These quantities are then converted to the cylindrical coordinates used as the initial conditions for the ray tracing equations. It is convenient to specify the initial poloidal mode number, m, even though toroidicity implies that it is not constant for a given ray. The boundary condition on the equations is that whenever the ray reaches the edge of the plasma, it is specularly reflected with loss. This reflection loss is used as the parameter to simulate power loss due to other mechanisms (such as unconfined energetic ions) which have been observed in the experiments but which have not been properly accounted for in the present theory.

Because we assume a fast equilibration over a flux surface, we need only

calculate the wave energy density averaged over a flux surface and not the local electric field strength. Thus we only solve the relatively simple equation for the power P (see below) rather than the more complicated field focusing equation which involves second derivatives of D.[8]

C. Wave absorption

In addition to the position and wavenumber, each ray is characterized by a power P (with units of watts). The differential equation for P is derived by calculating the power lost to the plasma by quasilinear diffusion.

On a given flux surface, a single ray contributes

$$U = P/(|v_{gr}|A)$$

to the wave energy density averaged over a flux surface where A is the area of the flux surface and v_{gr} is the radial component of the group velocity. The wave polarization is obtained from the relation $\bar{D}\cdot\vec{E}$ where $\bar{D}$ is the dispersion tensor of the plasma medium derived from the fluid equations. Its determinant D is used in the ray tracing calculation. Making use of

$$U = \frac{1}{4}\,\varepsilon_o\,\omega\,\vec{E}^{*}\cdot\frac{\partial\bar{D}}{\partial\omega}\cdot\vec{E} \quad ,$$

we can find the rms field strength due to the ray in terms of P. We now form the contribution of this ray to the quasilinear diffusion coefficient for particles of species s. From Kennel and Engelmann,[6] we have

$$\bar{D}_{ql,s} = \sum_n \frac{\pi}{2}\frac{q_s^2}{m_s^2}\,\delta(\omega - k_\parallel v_\parallel - n\,\Omega_s)\vec{a}_n\,\vec{a}_n$$

where

$$\vec{a}_n = \theta_n \frac{k_\parallel}{\omega}\left[\left(\frac{\omega}{k_\parallel} - v_\parallel\right)\hat{e}_\perp + v_\perp \hat{e}_\parallel\right]$$

$$\theta_n = \frac{E_r J_{n+1} + E_\ell J_{n-1}}{\sqrt{2}} + \frac{v_\parallel}{v_\perp} J_n E_\parallel \quad .$$

Here $\parallel$ and $\perp$ are measured with respect to the magnetic field, $E_{\ell,r}$ are the left- and right-handed components of the electric field, and the argument of the Bessel functions is $k_\perp v_\perp/\Omega_s$. The wave power absorbed per unit volume (Wm^{-3}) is

$$P_d = -\sum_s \int d^3\vec{v}\, n_s m_s \vec{v} \cdot \bar{D}_{ql,s} \cdot \frac{\partial f_s}{\partial \vec{v}} \quad .$$

Here n_s and m_s give the number density and mass of species. The distribution function f_s is normalized so that its velocity integral is unity.

Since f_s is taken to be isotropic, the three-dimensional integral collapses to one dimension. In the process, the δ functions appearing in the definition of $\bar{D}_{ql,s}$ become piecewise algebraic functions which are easily handled on a discrete grid. Finally, we utilize energy conservation to write down the equation for evolution of the power as

$$\frac{dP}{dt} = -P_d |v_{gr}| A \quad .$$

The rf damping is calculated in this way including all plasma species. However, the Fokker-Planck equation is only solved for the test species which dominate the wave absorption. For all the "background" species, the distributions are assumed to be Maxwellian and an analytical form (involving

the plasma dispersion function) for the rf damping rate can be obtained. Since the quasilinear diffusion tensor includes all resonance interaction, our approach has the advantage of treating all species and all collisionless damping processes in a uniform and easily understood manner. There do not have to be separate formulas for cyclotron and Landau damping, for example.

The power absorption for each species, p_{ds}, and quasilinear diffusion coefficient, $\bar{\bar{D}}_{ql,s}$ are accumulated as a function of radius, r. $\bar{\bar{D}}_{ql,s}(r)$ is used to advance the Fokker-Planck equation. The sum of p_{ds} and all collisional heating of the "background" species is input into BALDUR as a heating profile, while only p_{ds} is used if the Fokker-Planck equation for species s is not advanced. Because a single ray may cross a flux surface several times, $\bar{\bar{D}}_{ql,s}(r)$ involves a sum both over the rays and over the crossings.

D. Evolution of f_s

After all the ray tracing calculations are completed, we may advance f_s by solving the Fokker-Planck equation. Although f_s may be computed for all the species, it is usually necessary to do so for those species which depart significantly from a Maxwellian. In the minority heating case, for example, this normally includes only the minority ions.

For each test species, s, and for each radial zone we solve the isotropic Fokker-Planck equation

$$\frac{\partial f_s}{\partial t} = \frac{\partial f_s}{\partial t}\bigg|_{coll} + \frac{1}{v^2}\frac{\partial}{\partial v} v^2 D_{ql,s} \frac{\partial}{\partial v} f_s$$

where $D_{ql,s}$ is the accumulated vv component of the quasilinear diffusion tensor provided by the ray tracing calculation. This equation is advanced by

a time interval equal to the time step used by BALDUR. In this phase of the calculation the collisional heating of the background species is also computed.

The collision term is calculated assuming all the background species are Maxwellians with temperature T_s. This requires some justification. The correct Fokker-Planck problem is one involving both velocity and configuration space. What we have done is to factor the problem into a velocity space part, which we solve here, and a configuration space part, which is converted to a diffusion equation and solved by the main part of BALDUR. Because BALDUR handles the terms leading to temperature equilibration between the various species, such terms should be excluded from the velocity-space problem. This is most conveniently done by making all the background temperatures equal. The power flows in the reduced problem then all arise from the rf heating. This approach will break down if a major component of the plasma (electrons or majority ions) becomes very non-Maxwellian, as may happen during second harmonic heating. Then the velocity-space calculation should use the real distributions and BALDUR should include the temperature equilibrium term.

Since f_s has now changed, we may wish to repeat the ray tracing calculation to determine new power deposition profiles. Similarly, we can repeat the solution of the Fokker-Planck equation using the new wave fields. Provision is made in the program for iterating this procedure an arbitrary number of times. However, in practice, no iteration is necessary because each time the code is executed the distribution function found in the previous call is used. As long as the BALDUR time step is sufficiently small, there will only be a small change in the distribution from one step to the next and little error is incurred.

E. Power budget

The power balance in this code is complicated by the fact that energy absorbed by the particles may be stored in the test species before collisionally transferring it to the background species (and BALDUR). An example will make this clearer.

Suppose we are simulating ^{3}He minority heating in a deuterium plasma. Let us take the helium to be a test species and the deuterium and electrons to be "background" species. Conceptually, it is useful to consider two helium distributions: the non-Maxwellian test distribution and the Maxwellian background distribution. During the ray tracing there may be some damping on all the species, although presumably most of the wave energy will damp on the minority helium. The energy which is damped on the electrons and deuterons is stored and later given to BALDUR as part of the heating term. The energy which is damped on the helium is computed from the quasilinear diffusion of the test distribution and goes to creating a tail in the helium test distribution function. This tail interacts with all the background species resulting in collisional heating of the electrons and deuterons. The collisional power transfer is added to the direct wave heating to provide the total electron and deuteron heating terms. Collisional heating is the only power source for the background helium ions. Finally the contributions for the deuterons and helium ions are added together to give a combined ion heating term, and the resulting ion and electron heating profiles are passed back to BALDUR. In this way the energy that is damped on the minority ions is reapportioned among the background species (if the minority tail is sufficiently energetic, most of its energy goes to the electrons). However, the sum of the collisional heating terms will only balance the minority wave heating term in the steady state. The difference between the minority wave

heating and the collisional heating causes the energy of the test minority distribution to change. This means that the collisional heating will only become effective some time into the rf heating pulse (when the minority tail is established). However, it will remain for some time after the rf is turned off while the tail relaxes back to a Maxwellian.

III. SIMULATION OF PLT EXPERIMENTAL RESULTS

The ICRF modeling code has been used extensively to simulate the heating results on PLT in the minority ion regime. In these experiments, both helium-3 and hydrogen have been used as the minority ion species in a deuterium plasma. The basic approach of the simulation is to use the power deposition profile produced by the rf code, and vary the transport model to obtain the best fit to the data. The same transport scaling has been used for the ohmic and the rf phase of the discharge.

In the experiments, the wave is launched using loop antennae extending half of the minor circumference of PLT on the outer major radius of the tokamak (see Fig. 1). The rf current distribution on the antennae has been computed for the two applied frequencies, 42 and 25 MHz. From the antenna power distribution, the poloidal mode spectrum is obtained. The initial toroidal mode spectrum is determined from the phasing of the various antennae located at different toroidal positions.

The propagation of the wave from the antenna to the plasma interior is represented typically by 30 to 50 rays distributed uniformly in the poloidal direction near the antenna surface. The total rf input power is divided among the rays according to their poloidal locations and the corresponding rf power profile excited by the antenna. In the experiments, the rf current maximum has been adjusted to be near the equatorial midplane of the tokamak, i.e., at

the center of the half-turn loop. The plasma parameters and profiles are given by BALDUR after a steady-state ohmic solution similar to the experimental conditions has been achieved.

The ray tracing process is illustrated in Fig. 2. Twenty rays have been launched at various poloidal angles from the low magnetic field region of the tokamak with different wave numbers (see figure caption). The plasma is composed of majority deuterons and 5% minority hydrogen ions. The applied frequency is 42 MHz, corresponding to the hydrogen cyclotron frequency at 28 kG. The toroidal transform in the plasma is determined with the specification of the q profile. For the example shown in Fig. 2, the q profile varies from 1 at the plasma center to ~ 4 at the limiter radius of 40 cm. The rays are reflected at the fast wave cutoff layers located in the plasma core and at the plasma periphery. Each cross superimposed on the rays represents the damping of 10% of the wave energy as computed from quasilinear theory.

The time evolution of the minority hydrogen distribution is shown in Fig. 3 where the initial 1 keV thermal ions have been heated to a non-Maxwellian tail. The tail distribution is slowing down on the electron population which is fixed at 1 keV.

For the ICRF heating simulation given below an antenna coupling efficiency of 90% is assumed so that ~ 1.1 MW of the total rf power of 1.2 MW reached the plasma. Approximately 900 kW of this power is damped on the minority ions, 100 kW is coupled directly to the background species, and about 100 kW is lost due to finite reflectivity at the cutoff region in the plasma periphery simulating power loss due to the unconfined high energy hydrogen tail. (In this simulation, the reflectivity was taken to be 90%.) The power splitting of the collisional interaction between the minority ions and the background species is 400 kW to the electrons, 500 kW to the deuterons.

A transport model which fits the experimental data well can be summarized as follows. The electron thermal conductivity, χ_e, takes the form of

$$\chi_e = \chi_{nc} + \frac{1.65 \times 10^{17}}{n_e(r)\left[T_e(r)/T_e(0)\right]^{1/2}}$$

where χ_{nc} is the neoclassical electron conduction and the $T_e(r)$ dependence enhances the conduction at the plasma edge above the usual Alcatorlike scaling. (These quantities are all expressed in CGS units.) The minority hydrogen radial density profile is adjusted to follow the n_e profile closely. The line averaged electron density time evolution is programmed to be similar to the experimental results through both gas puffing and recycling off limiters.

The particle diffusion coefficient has been chosen to match the electron density profiles for both the ohmic and rf heated plasma. The form of the diffusion coefficient, D_h, is

$$D_h = D_{nc} + 1000 + 0.05D_b + 5000\ (r/a)^3 \quad .$$

Here D_b is the Bohm diffusion and is included only inside the region where $q < 1$. Since the transport modeling of the central sawteeth activities observed in the experiments is not included in these studies, an enhanced conduction and diffusion coefficient, $0.05\ D_b$ is included to simulate the averaged T_e and n_e profiles over the sawteeth period inside $q = 1$. The ion conductivity is taken to be twice the Chang-Hinton neoclassical value.[9] The comparison of the $T_e(r)$ and $n_e(r)$ profile before and during the rf pulse with the Thomson

scattering data is shown in Figs. 4 and 7. The comparison of the central in temperature evolution is given in Fig. 8. The agreement between the simulation and the data is quite good although the transport model used is not unique.

The ICRF transport code has also been used to extrapolate the heating results to future tokamaks such as FED and INTOR. Studies of ICRF heating of FED with 26 MW of rf power with 10% hydrogen minority in a plasma composed of 45% deuterium and 45% tritium has been reported in trade study reports.[10] Furthermore, BALDUR has been used to estimate the ignition condition for a device like FED by scanning the rf power with constant pulse length, or varying the pulse length at constant power level. Examples of these scans are given in the design studies where the volume-averaged beta and T_i are plotted versus the pulse length and the power level. The antenna system used in these computations is still loop type. We are in the process of incorporating wave coupling calculations for other wave launchers, such as waveguides or slot cavities, into the transport code.

IV. CONCLUSION AND IMPROVEMENTS

The underlying constraint in the ICRF heating transport calculations presented here is the assumption that wave propagation and absorption are correct, and the transport model or the rf power level is iterated to match the experimental data. With the approximations in the rf model, such as fluid wave polarization and isotropic distributions, the resultant transport model is consistent with the ohmic value. Further improvements of the wave model and the treatment of the energetic particles can facilitate better understanding of the heating physics. Several of these modifications are under way while others require better approximations to meet the limits on

computer time.

The antenna coupling problem for different launchers, which may be relevant for future devices, needs to be addressed. For loop antenna, the wave coupling is only weakly sensitive to the plasma profiles; thus it is only necessary to calculate the antenna field pattern once initially. So far the wave coupling in a cold plasma has been used. The temperature effects on these calculations remain to be assessed.

A better treatment of the wave polarization in a hot plasma and in regions where WKB solutions become invalid needs to be developed. Ray tracing calculation in a finite plasma is under investigation. In the ion-ion hybrid mode conversion regime, the WKB treatment becomes invalid; thus a full wave solution is necessary to derive the fields inside the zone between the cutoff and the mode conversion layers. Several techniques which have been developed for one-dimensional plane wave solution[11] are being generalized to the two-dimensional problem.

In the experiments, the energetic minority tail has been observed to be anisotropic in velocity space. Moreover, these particles can follow trapped particle orbits which so far have been neglected in our computations. There are several approaches depending on the specific area of interest for the energetic particle problem. If the main interest is to calculate the velocity space anisotropy, a two-dimensional Fokker-Planck treatment can be used. However, this computation is too slow for interfacing with any transport code. It may be possible to retain the important physics by considering only a few Legendre harmonics of f. If the objective is to study the transport and confinement properties of these particles, Monte Carlo techniques can be employed. Again this is a very time consuming process and difficult to couple with a transport calculation. A better approach is to compute the

neoclassical transport coefficients for the non-Maxwellian anisotropic distributions which can be easily incorporated into the transport model. This way the energetic species can be treated the same as the background plasma components. This is especially important for second harmonic heating where the majority ion species is non-Maxwellian and anisotropic.

ACKNOWLEDGMENTS

The authors would like to thank F. W. Perkins, D. E. Post, D. R. Mikkelsen, and A. E. Silverman for useful discussions and the BALDUR group for their help in implementing the code. This work was supported by the U.S. Department of Energy Contract No. DE-AC02-76-CHO-3073.

REFERENCES

[1] J. Hosea et al., Phys. Rev. Lett. 43, 1802 (1979).

[2] D. Q. Hwang et al., in Proceedings of the Ninth International Conference on Plasma Physics and Controlled Nuclear Fusion Research, Baltimore, MD, 1982, IAEA-CN-41/I-1.

[3] Equipe TFR, in Proceedings of the Ninth International Conference on Plasma Physics and Controlled Nuclear Fusion Research, Baltimore, MD, 1982, IAEA-CN-41/I-2.

[4] H. Kimura et al., in Proceedings of the Ninth International Conference on Plasma Physics and Controlled Nuclear Fusion Research, Baltimore, MD, 1982, IAEA-CN-41/J-3.

[5] T. Amano et al., in Proceedings of the Ninth International Conference on Plasma Physics and Controlled Nuclear Fusion Research, Baltimore, MD, 1982, IAEA-CN-41/C-3.

[6] C. F. Kennel and F. Engelmann, Phys. Fluids 9, 2377 (1966).

[7] C. F. F. Karney, D. Q. Hwang, and J. M. Hovey, Bull. Phys. Soc. 26, 929 (1981).

[8] I. B. Bernstein, Phys. Fluids 18, 320 (1975).

[9] C. S. Chang and F. L. Hinton, Phys. Fluids 9, 1493 (1982).

[10] C. A. Flanagan et al., Oak Ridge National Laboratory Report No. ORNL/TM-7949/VI, p. 2-24.

[11] D. E. Swanson, Phys. Fluids 21, 926 (1978).

FIGURE CAPTIONS

FIG. 1 Geometry of the PLT antenna used in the ICRF heating experiments. The antenna is located at 43 cm of the minor radius. The poloidal rf current distributions correspond to waves at 25 MHz (solid) and 42 MHz (dashed).

FIG. 2 Rays representing the rf power flow from the antenna to the plasma core around 20 poloidal locations. The rays correspond to a wave vector of n = toroidal mode number = 5, m = poloidal mode numbers = 1,0, and -1. The power distribution of the rays is given by the antenna geometry and coupling. The plasma mixture is 80% D, 5% H, and Z_{eff} of 1.5, C and Ti impurities.

FIG. 3 The time evolution of hydrogen minority ion distribution produced by the rf heating at the plasma center. The initial Maxwellian distribution is the bulk plasma temperature.

FIG. 4 Comparison of the computed equalibrium electron density profile from the transport code and the exprimental data from Thomson scattering during ohmic discharge. The particle diffusion coefficient is $D_h = D_{nc} + 1000 + 0.05\ D_b + 5000\ (r/a)^3$ where D_b is Bolm diffusion inside q < 1 region.

FIG. 5 Comparison of the ohmic electron temperature profiles between transport code and data with

$$\chi_e = \chi_{nc} + \frac{1.65 \times 10^{17}}{n_e(r)\ \left(T_e(r)/T_e(0)\right)^{1/2}} .$$

FIG. 6 Comparison of $n_e(r)$ profile near the end of the rf pulse using the same transport model.

FIG. 7 Comparison of $T_e(r)$ profile near the end of the rf pulse.

FIG. 8 Comparison of the time evolution of the central ion temperature between transport calculation and data values deduced from neutron flux.

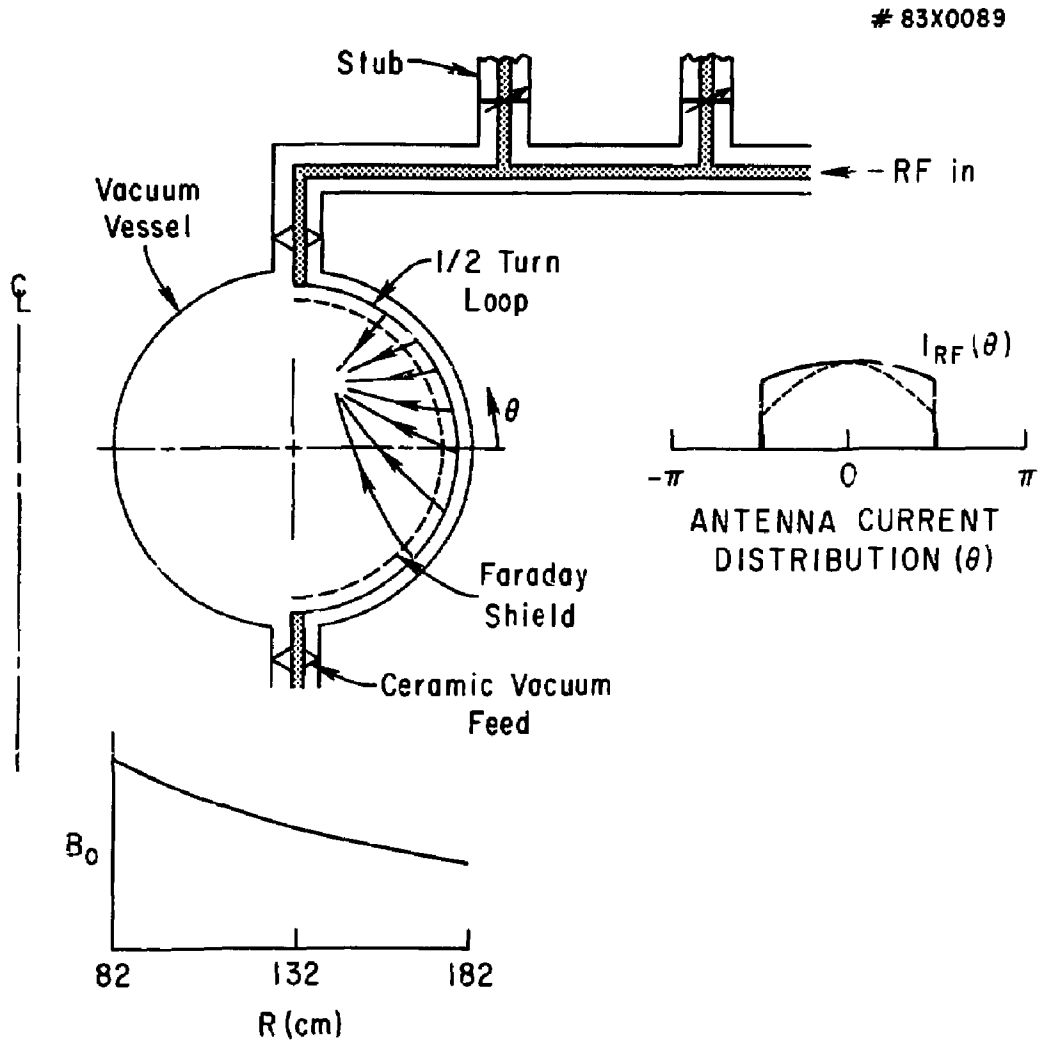
83X0089
Stub
RF in
Vacuum Vessel
1/2 Turn Loop
θ
Faraday Shield
Ceramic Vacuum Feed
$I_{RF}(\theta)$
$-\pi$
0
π
ANTENNA CURRENT DISTRIBUTION (θ)
B_0
82
132
182
R (cm)

Fig. 1

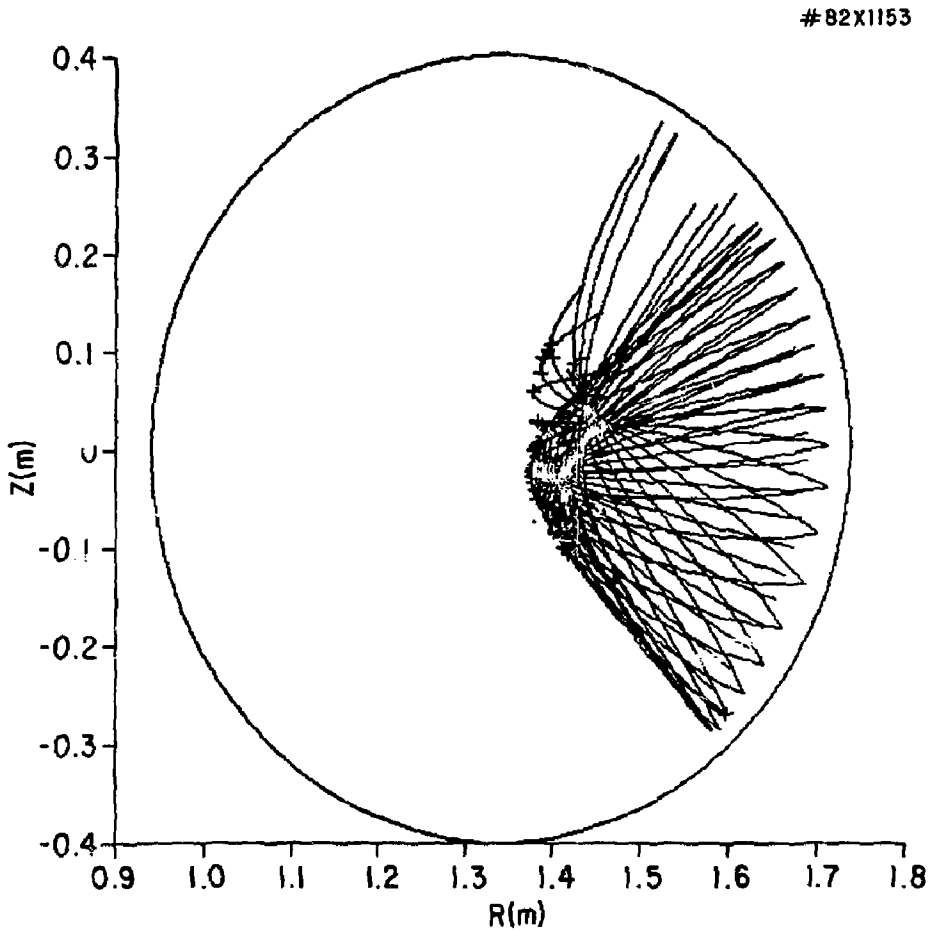

Fig. 2

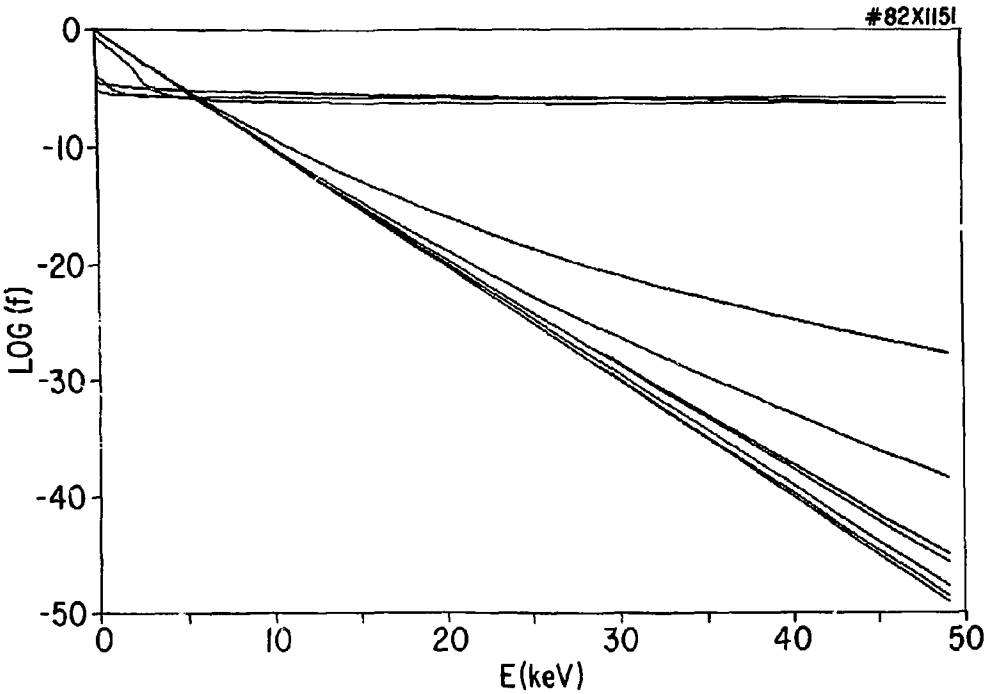

Fig. 3

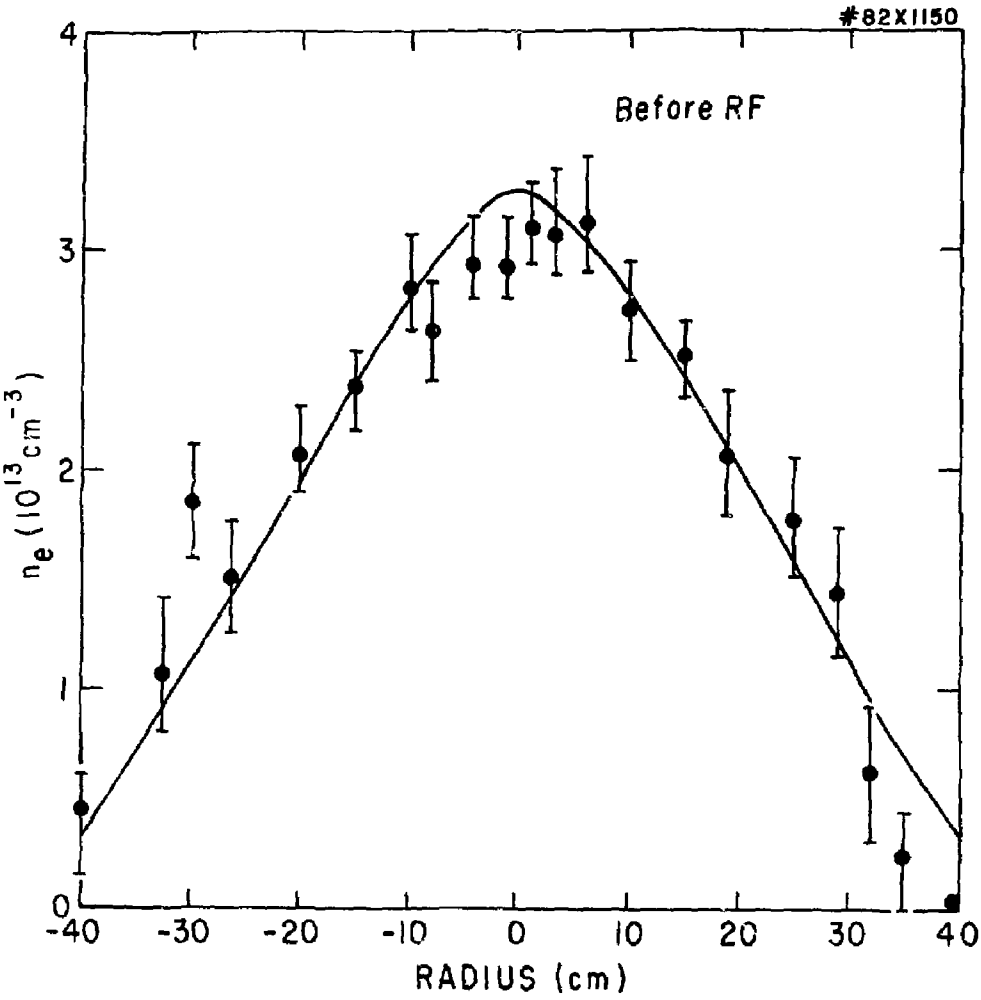
#82X1150
Before RF
n_e (10^{13} cm^{-3})
0
1
2
3
4
-40
-30
-20
-10
0
10
20
30
40
RADIUS (cm)

Fig. 4

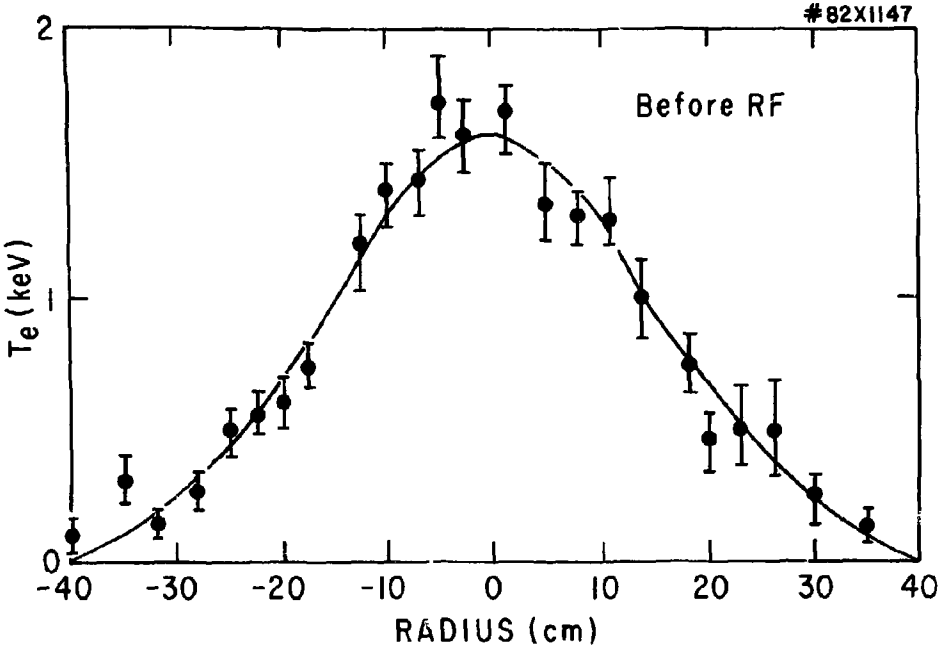

Fig. 5

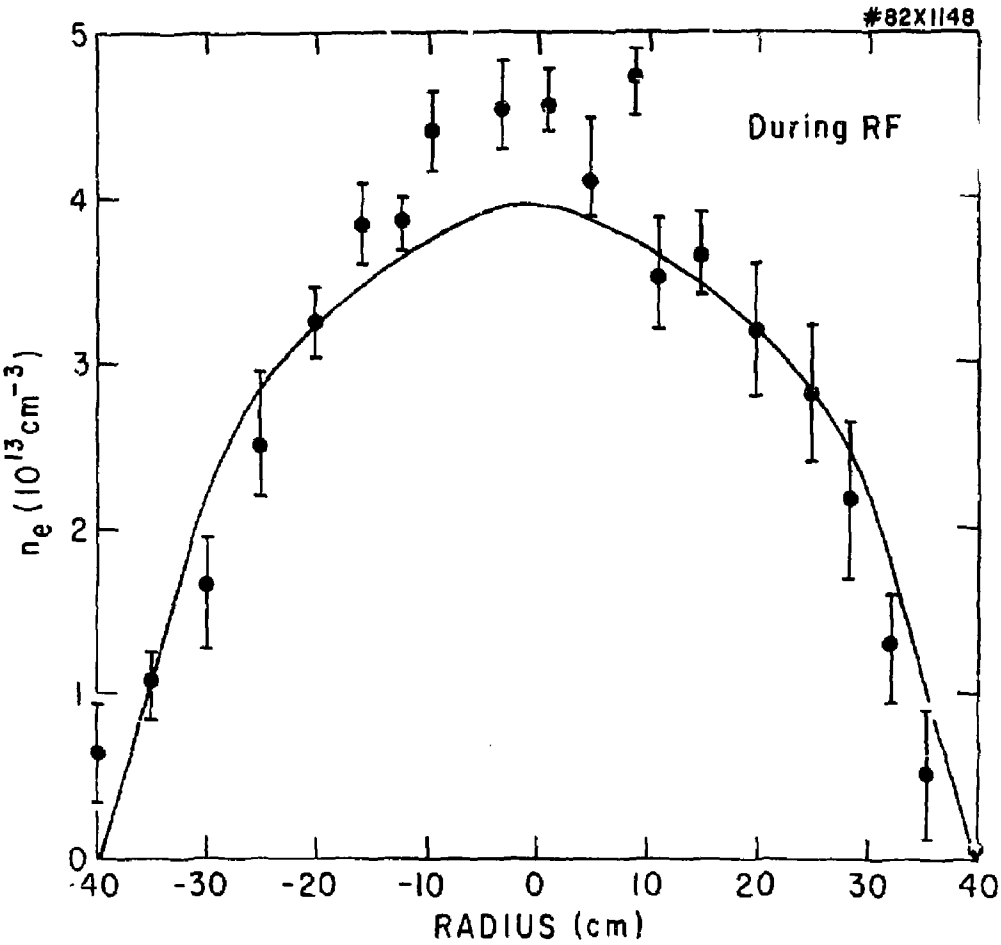
#82X1148
During RF
n_e (10^{13}cm^{-3})
RADIUS (cm)
0
1
2
3
4
5
-40
-30
-20
-10
0
10
20
30
40

Fig. 6

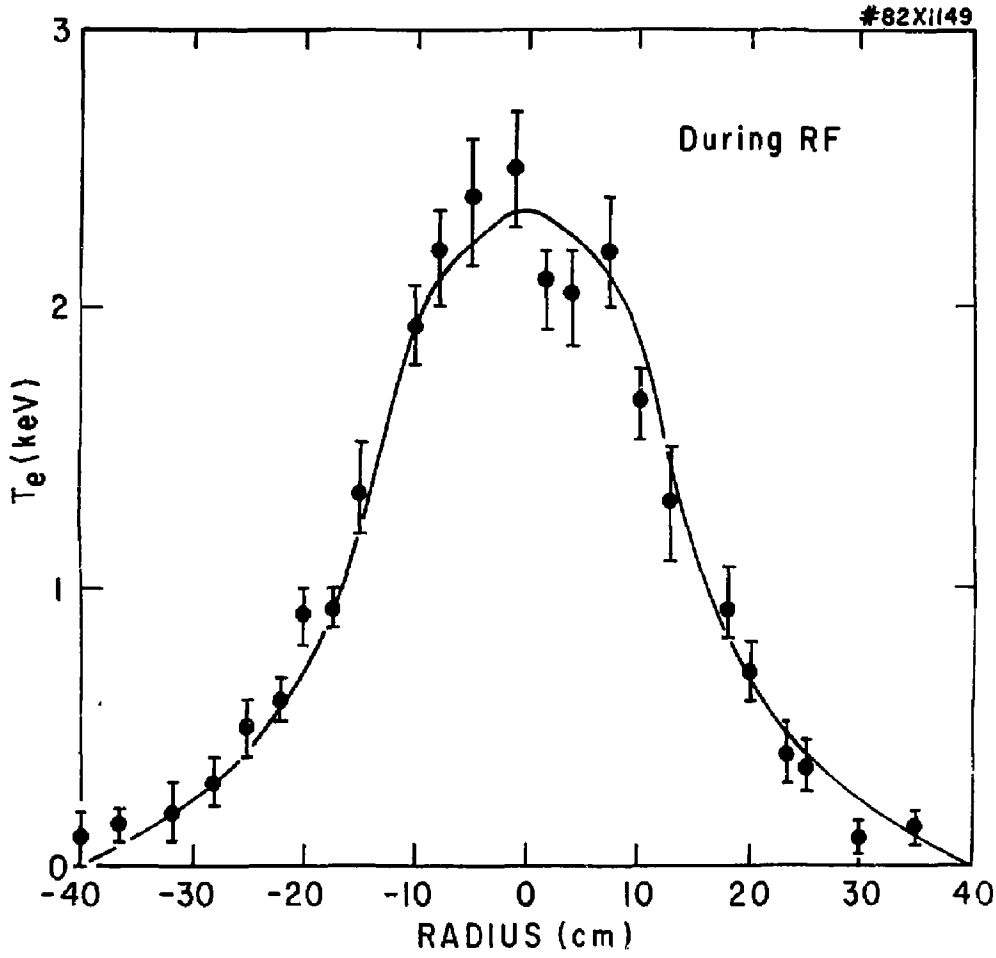

Fig. 7

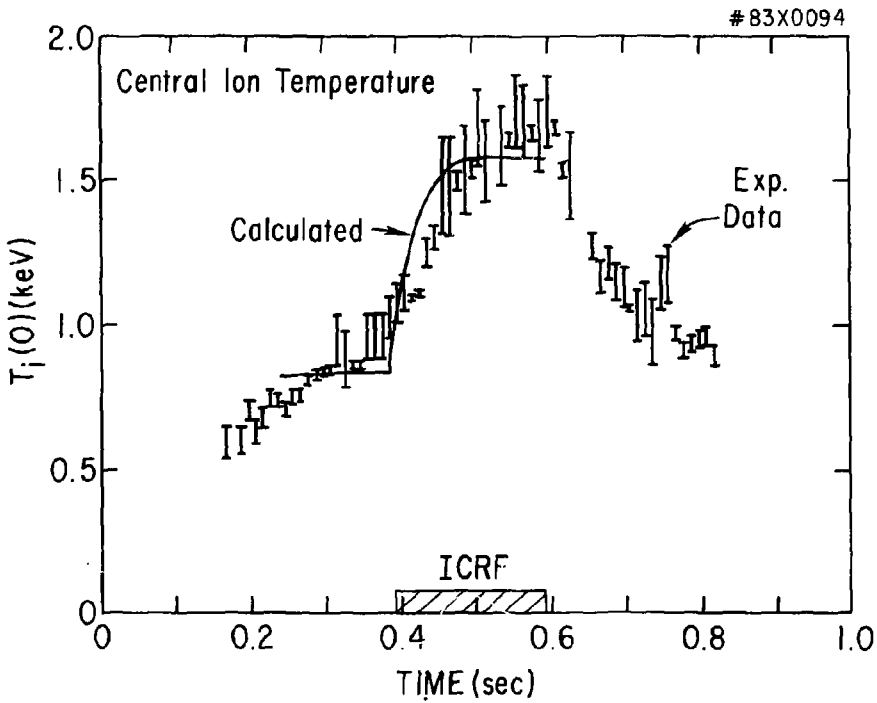
#83X0094
Central Ion Temperature
Calculated
Exp.
Data
ICRF
$T_i(0)$(keV)
TIME (sec)
2.0
1.5
1.0
0.5
0
0.2
0.4
0.6
0.8
1.0

Fig. 8

EXTERNAL DISTRIBUTION IN ADDITION TO TIC UC-20

Plasma Res Lab, Austra Nat'l Univ, AUSTRALIA
Dr. Frank J. Paoloni, Univ of Wollongong, AUSTRALIA
Prof. I.R. Jones, Flinders Univ., AUSTRALIA
Prof. M.H. Brennan, Univ Sydney, AUSTRALIA
Prof. F. Cap, Inst Theo Phys, AUSTRIA
Prof. Frank Verheest, Inst theoretische, BELGIUM
Dr. D. Palumbo, Dg XII Fusion Prog, BELGIUM
Ecole Royale Militaire, Lab de Phys Plasmas, BELGIUM
Dr. P.H. Sakanaka, Univ Estadual, BRAZIL
Dr. C.R. James, Univ of Alberta, CANADA
Prof. J. Teichmann, Univ of Montreal, CANADA
Dr. H.M. Skarsgard, Univ of Saskatchewan, CANADA
Prof. S.R. Sreenivasan, University of Calgary, CANADA
Prof. Tudor W. Johnston, INRS-Energie, CANADA
Dr. Hannes Barnard, Univ British Columbia, CANADA
Dr. M.P. Bachynski, MPB Technologies, Inc., CANADA
Zhengwu Li, SW Inst Physics, CHINA
Library, Tsing Hua University, CHINA
Librarian, Institute of Physics, CHINA
Inst Plasma Phys, SW Inst Physics, CHINA
Dr. Peter Lukac, Komenskeho Univ, CZECHOSLOVAKIA
The Librarian, Culham Laboratory, ENGLAND
Prof. Schatzman, Observatoire de Nice, FRANCE
J. Radet, CEN-BP6, FRANCE
AM Dupas Library, AM Dupas Library, FRANCE
Dr. Tom Nual, Academy Bibliographic, HONG KONG
Preprint Library, Cent Res Inst Phys, HUNGARY
Dr. A.K. Sundaram, Physical Research Lab, INDIA
Dr. S.K. Trehan, Panjab University, INDIA
Dr. Indra, Mohan Lal Das, Banaras Hindu Univ, INDIA
Dr. L.K. Chavda, South Gujarat Univ, INDIA
Dr. R.K. Chhajlani, Var Ruchi Marg, INDIA
P. Kaw, Physical Research Lab, INDIA
Dr. Phillip Rosenau, Israe Inst Tech, ISRAEL
Prof. S. Cuperman, Tel Aviv University, ISRAEL
Prof. G. Rostagni, Univ Di Padova, ITALY
Librarian, Int'l Ctr Theo Phys, ITALY
Miss Clelia De Palo, Assoc EURATOM-CNEN, ITALY
Biblioteca, del CNR EURATOM, ITALY
Dr. H. Yamato, Toshiba Res & Dev, JAPAN
Prof. M. Yoshikawa, JAERI, Tokai Res Est, JAPAN
Prof. T. Uchida, University of Tokyo, JAPAN
Research Info Center, Nagoya University, JAPAN
Prof. Kyoji Nishikawa, Univ of Hiroshima, JAPAN
Prof. Sigeru Mori, JAERI, JAPAN
Library, Kyoto University, JAPAN
Prof. Ichiro Kawakami, Nihon Univ, JAPAN
Prof. Satoshi Itoh, Kyushu University, JAPAN
Tech Info Division, Korea Atomic Energy, KOREA
Dr. R. England, Ciudad Universitaria, MEXICO
Bibliotheek, Fom-Inst Voor Plasma, NETHERLANDS
Prof. B.S. Liley, University of Waikato, NEW ZEALAND
Dr. Suresh C. Sharma, Univ of Calabar, NIGERIA
Prof. J.A.C. Cabral, Inst Superior Tech, PORTUGAL
Dr. Octavian Petrus, ALI CUZA University, ROMANIA
Dr. R. Jones, Nat'l Univ Singapore, SINGAPORE
Prof. W.A. Hellberg, University of Natal, SO AFRICA
Dr. Johan de Villiers, Atomic Energy Bd, SO AFRICA
Dr. J.A. Tagle, JEN, SPAIN
Prof. Hans Wilhelmson, Chalmers Univ Tech, SWEDEN
Dr. Lennart Stenflo, University of UMEA, SWEDEN
Library, Royal Inst Tech, SWEDEN
Dr. Erik T. Karlson, Uppsala Universitet, SWEDEN
Centre de Recherchesen, Ecole Polytech Fed, SWITZERLAND
Dr. W.L. Weise, Nat'l Bur Stand, USA
Dr. W.M. Stacey, Georg Inst Tech, USA
Dr. S.T. Wu, Univ Alabama, USA
Prof. Norman L. Oleson, Univ S Florida, USA
Dr. Benjamin Ma, Iowa State Univ, USA
Prof. Magne Kristiansen, Texas Tech Univ, USA
Dr. Raymond Askew, Auburn Univ, USA
Dr. V.T. Tolok, Kharkov Phys Tech Ins, USSR
Dr. D.D. Ryutov, Siberian Acad Sci, USSR
Dr. M.S. Rabinovich, Lebedev Physical Inst, USSR
Dr. G.A. Eliseev, Kurchatov Institute, USSR
Dr. V.A. Glukhikh, Inst Electro-Physical, USSR
Prof. T.J. Boyd, Univ College N Wales, WALES
Dr. K. Schindler, Ruhr Universitat, W. GERMANY
Nuclear Res Estab, Julich Ltd, W. GERMANY
Librarian, Max-Planck Institut, W. GERMANY
Dr. H.J. Kaeppler, University Stuttgart, W. GERMANY
Bibliothek, Inst Plasmaforschung, W. GERMANY